

Synthetic Biology Meets Neuromorphic Computing: Towards a Bio-Inspired Olfactory Perception System

Kevin Max^{1,2}, Larissa Sames³, Shimeng Ye⁴, Jan Steinkühler^{3,5},
and Federico Corradi⁴

¹Neural Computation Unit, Okinawa Institute of Science and Technology, Japan

²Department of Physiology, Bern University, Switzerland

³Bio-Inspired Computation, Institute of Electrical and Information Engineering, Kiel University, Kiel, Germany

⁴Electrical Engineering, Eindhoven University of Technology, The Netherlands

⁵Kiel Nano, Surface and Interface Science KiNSIS, Kiel University, Kiel, Germany

E-mail: kevin.max@oist.jp, jst@tf.uni-kiel.de, f.corradi@tue.nl

Keywords: neuromorphic engineering, olfaction, chemical sensing, synthetic biology

Abstract. In this study, we explore how the combination of synthetic biology, neuroscience modeling, and neuromorphic electronic systems offers a new approach to creating an artificial system that mimics the natural sense of smell. We argue that a co-design approach offers significant advantages in replicating the complex dynamics of odor sensing and processing. We investigate a hybrid system of synthetic sensory neurons that provides three key features: a) receptor-gated ion channels, b) interface between synthetic biology and semiconductors and c) event-based encoding and computing based on spiking networks. This research seeks to develop a platform for ultra-sensitive, specific, and energy-efficient odor detection, with potential implications for environmental monitoring, medical diagnostics, and security.

1. Introduction

Biological olfaction is a remarkably efficient sensory system, surpassing engineered chemical detection methods through redundant neural circuits that ensure robust responses [1], combinatorial coding that enables the detection of thousands of odors [2, 3], and exceptional sensitivity [4]. These advantages have inspired extensive efforts to replicate biological olfaction, leading to significant improvements in artificial olfaction. Today's electronic noses (e-noses) and artificial olfactory biosensors employ arrays of chemosensors and advanced pattern recognition algorithms, enabling odor classification in an impressive variety of fields, from biomedical signal analysis [5] and environmental monitoring [6], to food safety [7], agricultural productivity [8], and security [9].

Despite these notable achievements, e-nose technologies continue to face several key challenges that have slowed their broader adoption. These include: (i) sensor drift, which deteriorates performance over time [10]; (ii) cross-sensitivity, which leads

to reduced specificity when sensors respond to multiple volatile compounds [11, 12]; (iii) significant power consumption [13], hampering the feasibility of portable or embedded deployments [12]; (iv) limited computational capacity for interpreting the complex combinatorial patterns inherent in real-world odors [14]; and (v) insufficient adaptability, as current systems cannot dynamically refine their responses from experience, unlike their biological counterparts [4]. Observing how biological olfaction circumvents these problems suggests a promising model for the next generation of artificial olfactory devices, particularly given its robust signal processing capabilities, cross-selective receptor integration, and the ability to learn from repeated exposure [14–16].

A striking feature of biological olfaction is its capacity to handle the vast complexity of real-world odors. In nature, few odorants appear in isolation and unpredictable interactions among volatile compounds often challenge artificial sensors. In contrast, humans, for example, can distinguish an astonishing large number of odors; an early estimate puts the number around 10,000, although subsequent studies point to a significantly higher figure (albeit with some debate) [17, 18].

Crucially, olfactory receptors do not respond to each odorant in isolation; instead, volatile compounds compete for overlapped receptor sites through a process often described as odor occlusion [19, 20]. These competitive interactions can be highly non-linear: one odorant can amplify receptor activity, while another can dampen it, leading to outcomes that defy simple additive models [20]. Such receptor-level dynamics introduce yet another layer of complexity, making biological olfaction remarkably adept at navigating real-world odor spaces. Unlocking these principles in engineered systems promises to push artificial olfaction beyond its current limits, paving the way for more robust, adaptable, and context-aware sensing technologies.

1.1. Background & state-of-the-art

1.1.1. Sensing technology. Bioinspired artificial olfactory systems use various sensing technologies, including metal oxide semiconductors, conductive polymers, and integrated MEMS sensor arrays [21–23]. These systems operate by detecting changes in physical properties, primarily electrical conductance, when volatile compounds interact with sensing materials. Discriminatory power is achieved through differential molecular interactions between multiple sensors and pattern recognition of the resulting combinatorial responses [13, 23–26].

Metal oxide sensors, while effective for chemical detection, face significant drift that compromises their long-term reliability and applicability in the real world [27, 28]. This drift manifests as temporal shifts in sensor response under identical working conditions, primarily caused by chemical and physical interactions at the sensing film microstructure, as well as external factors such as temperature and humidity variations. For example, recent analysis of the widely used gas sensor dataset by Vergara et al. [29] revealed how sensor drift can significantly affect recordings, hindering realistic

assessment of sensor performance [28]. Although traditional approaches attempt to address drift through regression models and environmental compensation [30, 31], bio-inspired neuromorphic implementations offer promising alternatives through spike-based encoding [32] and adaptive learning mechanisms that could potentially provide stability and resistance to drift [33]. These neuromorphic approaches aim to reduce the complexity of the data and implement adaptive algorithms that can follow changing conditions, potentially offering a more robust solution to the persistent challenge of sensor drift.

Building on these concepts, integrated analog on-chip learning circuitry has demonstrated efficacy in odor detection and classification. For example, Covington et al. in [24] used an 80 element chemoresistive microsensor array combined with a microfluidic package, while Tang et al. in [26] relied on commercially available sensors and a traditional signal processing pipeline in a microprocessor to distinguish three fruit fragrances. In a related work [25], Bernabei et al. utilized a large array of chemosensors with slightly varied sensor elements to emulate the overlap selectivity characteristic of biological olfaction, generating rich combinatorial responses. More recently, Rastogi et al. [34] introduced a neuromorphic analog e-nose that directly encodes the gas concentration using metal oxide (MOx) sensors and an analog front-end that transforms sensor responses into spike-based representations. Their approach leverages the time difference between spikes in two distinct processing pathways to infer gas concentration, reducing data redundancy, and improving power efficiency.

However, current polymer and metal oxide-based sensing elements remain relatively simple compared to biological olfactory systems, facing challenges with odor specificity and stability [11, 35]. Although these artificial sensors can detect certain volatile compounds, they often require high operating temperatures and exhibit limited effectiveness in discriminating complex molecular mixtures [36]. Moreover, their continuous sampling needs and high power consumption stand in stark contrast to the low-power, event-driven nature of biological olfaction [4]. These fundamental discrepancies in functionality and energy efficiency highlight the limitations of conventional chemosensors in achieving the richness and adaptability seen in biological odor detection.

Compared to traditional chemosensors, biosensors directly interface with a biological element, such as a whole cell or a purified protein, which is then linked to a physical transducer [37]. Although harnessing authentic biological receptors offers the potential for greater specificity, it also brings practical hurdles, including potentially shorter operating lifetimes, contamination risks, and more complex maintenance requirements. A promising alternative is to adopt a bottom-up synthetic biology strategy that extracts specific components of the olfactory system, like receptor proteins, and deploys them in controlled, nonliving environments. For example, reconstitution of mammalian and insect olfactory receptor proteins into stable platforms has been achieved in combination with electrical, optical, and acoustic signal transduction methods [38]. However, early efforts often focused on single receptors in isolation, which

failed to leverage the amplification cascades inherent to living cells.

Notably, some more recent works have demonstrated a more complete reconstitution of the olfactory system, in particular, into bio-mimetic environments, for example membrane bound vesicles formed by membrane extraction, or virus-like particles [39–42]. These approaches leverage the fact that insect olfaction is largely based on multivalent interactions between the conserved co-receptor Orco and the odorant binding subunits (odorant receptors, ORs), which together form a ligand-gated ion channel. Khadka et al. have demonstrated successful insertion of multiple odorant receptors into surface-anchored lipid vesicles. Yamada et al. [42] have demonstrated parts per billion sensitivity of an Orco-OR complex inserted into a lipid bilayer to octenol, a biomarker in human breath. Detection of femtomolar concentrations of VUAA1, E2-hexenal, 4-ethylguaiaicol molecules was demonstrated using odorant receptors Or10a, Or22a, and Or71a [41].

These studies show the feasibility of reconstituting functional and highly sensitive insect ORs in a non-living minimal system with electrical readout. However, none of these works have considered the multiplexed decoding signal from multiple ORs, the hallmark of the olfactory system. Additionally, previously used transducers, e.g. impedance spectroscopy, require energy-intensive sampling, and thus do not fully harness the event-driven character and amplification capabilities of biological olfaction.

1.1.2. Decoding algorithms for odor discrimination. The signal restoration challenge is being recognized as one of the central problems in neuromorphic olfaction [4, 43, 44]. In fact, for more than 20 years, researchers have concluded that the speed and accuracy of odor recognition in insects cannot be attributed solely to the performance of olfactory receptors due to their slow time constant and high variability [45]. The requirement to correctly classify odor concentrations poses additional demand on the analyzing algorithms, as do signal occlusion and noise effects. Thus, several models of signal processing downstream of the sensor have been investigated, e.g. [16, 45–53]. Methods for odor signal analysis can be broadly categorized into two classes: data analysis tools (e.g., principal component analysis, support vector machines) and biorealistic network models. While data analysis tools have been used for odor classification since many years [46, 47], biologically realistic network models are now studied with the goal of reaching the accuracy and efficiency of the animal olfactory system [16, 50–52]. Many of these models perform classification using a spatiotemporal code while learning in an unsupervised fashion. Additionally, some studies attribute the efficiency of natural systems to two main intrinsic mechanisms of biorealistic neural networks (i.e., Spiking Neural Network (SNN)): *i*) inhibition (which triggers a winner-takes-all competition [16, 48, 50]) and *ii*) temporal integration (due to neuron and network dynamics) [16, 45]. Recent work has also pursued the implementation of learning from teaching signals (supervised and reinforcement learning) in models of the insect olfactory system, in particular for associative learning [53, 54].

1.1.3. Neuromorphic implementation of olfactory models. Several hardware implementations have been demonstrated in digital Field Programmable Gate Arrays (FPGA) hardware [50], digital neuromorphic devices [16] and analog neuromorphic chips [23, 34, 48, 55]. Recently, a bio-realistic network [16], based on the architecture of the mammalian olfactory bulb, was implemented on the Loihi neuromorphic digital chip, demonstrating the benefits of employing an algorithm based on online learning and spike timing. However, the system was trained using a separately recorded data set of pure chemicals [29], therefore lacking integration with real chemosensors, and criticism has been raised regarding the generalizability of the network model [28].

The neuromorphic olfactory sensor literature indicates that there is considerable scope for improving neuromorphic chemosensory systems. There are several limitations in many of the current implementations, such as the lack of signal conditioning, the lack of integration of sensing and decoding in a single platform, high power consumption, and the poor sensitivity of the artificial sensor array. So far, the only truly integrated neuromorphic sensing platform for olfaction has been developed by Koickal et al. in 2006 [23, 56]. To our knowledge, this platform did not leave the proof-of-concept stage, and subsequent work by the authors has used conventional processing hardware [50]. This work is focused on integrating hardware realizations of all stages into one singular system.

2. Co-design of synthetic biology, bio-inspired models, and neuromorphic systems

A comprehensive approach is crucial in developing advanced neuromorphic chemosensory systems that effectively integrate sensor arrays, decoding algorithms, and their physical realization [57]. In this work, we present a novel methodology and preliminary results on how to move beyond the State-Of-The-Art (SOTA) by addressing the lack of codesign between these three components. Unlike previous chemical detection systems inspired by the olfactory pathway, which have treated sensing [47, 58], signal processing [59, 60], and neuromorphic computation [16] as separate components, our approach integrates these aspects to tackle the challenge of chemosensory perception in a comprehensive way. In this work, we introduce a new concept to couple the depolarization of synthetic cells made from biological materials directly with CMOS electronic circuits designed for spike generation, we call these new class of bio-electronic devices hybrid synthetic sensory neurons, and we depict them in Figure 1.

In doing so, our framework harnesses the advantages of co-design in a joint environment. Here, the three disciplines (neuroscience, synthetic biology, neuromorphic engineering) are developed together and connected to each other, as depicted in Figure 1:

- The bottom-up sensor design using synthetic biology informs the olfactory receptor (OR) and electrode response model, allowing us to simulate electrode responses with a biologically realistic ion channel model. In turn, this sets realistic estimates for electrode responses, which are crucial for the design of sensor and amplification

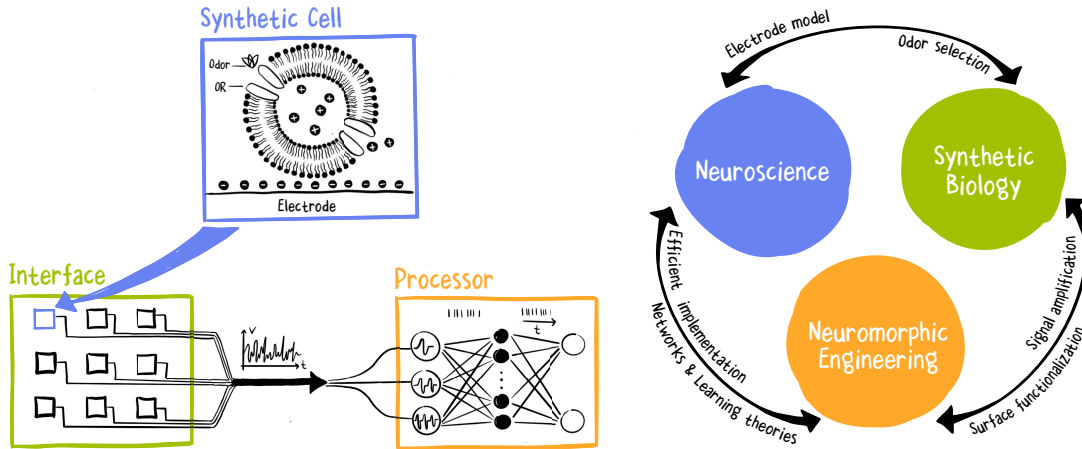


Figure 1: *Left*: Bio-inspired information flow from odor binding, depolarization of a synthetic cell, spike generation in a CMOS circuit (hybrid synthetic sensory neuron) and processing in a spiking neural network. *Right*: Co-design of SYNCH: “Combining SYnthetic Biology & Neuromorphic Computing for CHemosensory perception”, interconnecting the three disciplines of sensing with synthetic biology, efficient bio-inspired learning models, and neuromorphic hardware engineering.

stages. Importantly, this also allows us to pick Orco-OR complexes which respond strongly to the set of odor combinations that we aim to detect, while minimizing the number of required ORs which need to be deployed.

- The design of the sensor and neuromorphic processing stages are naturally intertwined: the bio-electro interface needs to be carefully selected and tuned (e.g. with regard to the electrode surface material, synthetic cell immobilization technique, geometry of sensor arrays, odorant flushing, and amplification electronics) to allow for optimal readout of the ionic currents, aiming for fast odorant throughput, high signal-to-noise ratio (SNR) and long lifetime of the immobilized synthetic cells.
- Computational theory and neuromorphic hardware in turn inform each other about how to realize energy-efficient olfactory processing and learning under real-life conditions. Theoretical ideas of few-shot, online learning in noisy environments can be tested on spiking hardware, and need to be made robust against constraints such as sparse coding and weight quantization. Here, a central issue is the compensation of sensor drift, which needs to be addressed by a theoretical approach, e.g. by a homeostatic learning mechanism inspired by biology, and then tested using the full sensor/processing hardware.

Our approach is not without challenges, as individual parts need to be optimized and tuned together but must still allow for the necessary flexibility. This

flexibility is needed as knowledge and research about the individual parts progresses simultaneously. The parallel approach is, on one hand, due to constraints of scientific funding—collaborative grants typically work on a common timeline from proposal to project end. However, parallelized development is also, in general, desired for time efficiency. As such, the collaborative tools we develop, particularly those that bridge data-driven synthetic biology with electrical and information engineering, not only represent standalone contributions to each field, but might also be useful in other applications.

3. Results & Discussions

3.1. Insect odor receptors provide a modular sensing platform

Insect olfaction is largely based on membrane-bound protein complexes consisting of an odorant receptor (OR) and a co-receptor, Orco. While ORs diverge in their sequence and odor specificity between the multitude of insects and the ecological niches they inhabit, the co-receptor Orco is highly conserved across insect species. Several experiments show that it is possible to create functional receptor complexes by combining Orco of one species with a foreign OR [61, 62]. From an engineering point of view, this suggests the possibility of a modular platform in which the base assembly of an Orco-based sensing element allows the swapping of ORs with different response profiles to target various compounds. To demonstrate this modularity, we set out to computationally assemble Orco-OR complexes using AlphaFold modeling [63, 64].

Specifically, we selected the Orco variant from the *D. melanogaster* (Dm) fruit fly and considered a total of 348 Orco-OR complexes, including non-Dm ORs. Each predicted Orco-OR structure was evaluated using the interface-predicted template modeling (ipTM) score, with higher values indicating greater confidence in the prediction accuracy of the protein-protein interface. An empirical cut-off point of 0.6 was chosen (Figure 2a1) [64, 65]. As expected, the positive control, consisting only of Orco-OR complexes from the same species (Dm), yielded mostly acceptable modeling outputs, as reflected in ipTM scores above 0.6. In contrast, the negative control, which used the mammalian OR from *M. musculus*, a receptor not expected to form a complex with Orco, did not produce any acceptable models (Figure 2a1). Interestingly, for Dm Orco and ORs from foreign species, we found a large fraction of potentially accurate models with ipTM scores above the 0.6 cut-off. This suggests that AlphaFold models are relevant for understanding the structures of Dm Orco in complex with ORs from foreign species.

To further evaluate the structures, we considered a second metric: interface solvation energy, which provides insight into the stability of the non-covalent binding between Orco and OR (Figure 2a2). More negative values indicate a more favorable binding interface [66]. We found that the obtained values for foreign OR were similar to those of the native Dm Orco-OR complexes (Figure 2b2), indicating comparable

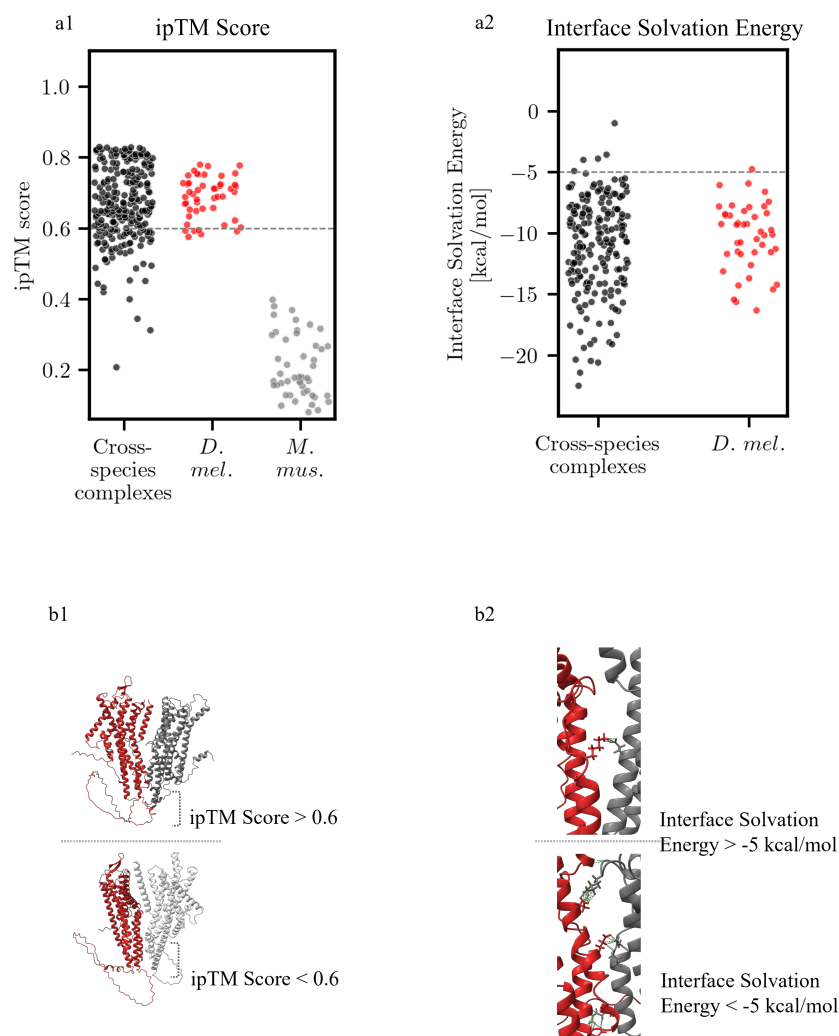


Figure 2: AlphaFold predictions suggest hundreds of possible stable complexes between *D. melanogaster* Orco and foreign odor receptors (OR). *a1*: AlphaFold ipTM score for Orco-OR complexes formed from *D. melanogaster* Orco combined with OR of different insect species (black), and combined with *D. melanogaster* (Dm) OR (positive control, red) and *M. musculus* OR (negative control, grey). *a2*: Interface solvation energy prediction for Dm with foreign OR above the ipTM cut-off of 0.6. Dashed grey lines indicates cut-off thresholds. *b1*: Dm Orco (red) dimerization with *M. sexta* OR4 resulted in an ipTM score above 0.6 (dark grey) while the dimerization with *L. migratoria* OR113 led to a score below 0.6 (grey). *b2*: Dm Orco and *B. mori* OR15 complex with favorable solvation energy (> -5 kcal/mol), whereas the dimerization with *C. quinquefasciatus* OR151 resulted in a low (< -5 kcal/mol) solvation energy. Varying number of bonds can be observed in the anchor domain (brackets). Green dashed lines indicate electrostatic interactions, while dashed blue lines represents hydrogen bonds.

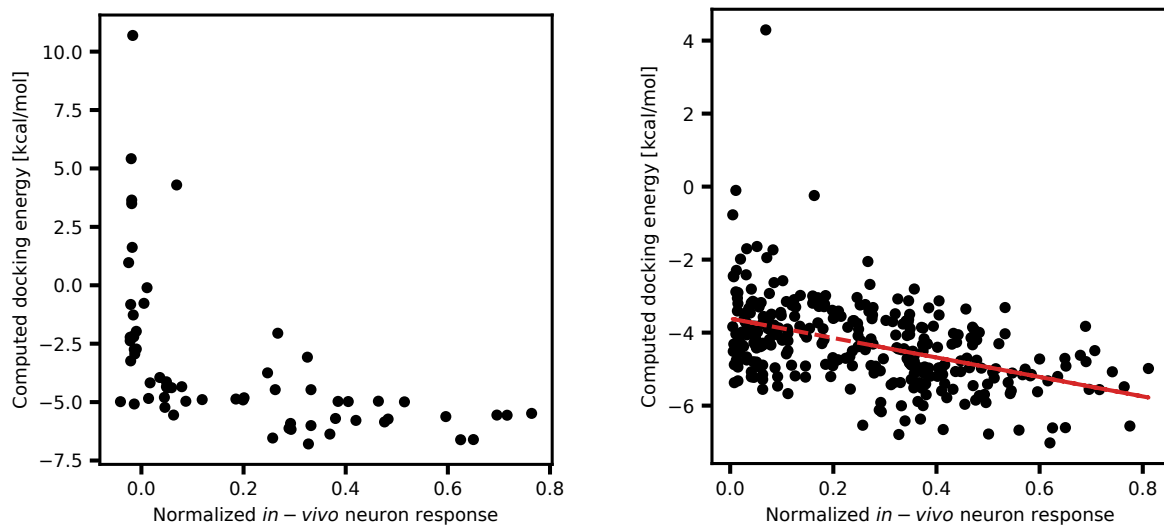


Figure 3: Comparison of ligand binding energies of Dm - Or69a, Or98a, Or19a and Or92a. Each datapoint corresponds to one odor molecule. Left: Terpene subset. Right: All odors from the DoOR dataset with positive neuron response. Dashed line shows linear regression with $R^2 = 0.2$

complex stability even for foreign ORs. Furthermore, we manually inspected the most favorable predictions for each group. In both cases, the interactions between the two subunits were confined to a segment of helical bundles stabilized by hydrogen bonds and electrostatic interactions located away the membrane interface (Figure 2a2), consistent with the anchor domain and interactions identified in experimental studies [67–69]. These results suggest that the OR structures generated by AlphaFold are promising candidates for computational exploration of the wide diversity of ORs.

To demonstrate the potential to build a digital representation of OR-odor interactions, we challenged the generated AlphaFold Orco-OR structures with *in-vivo* recordings of neuronal activity. We used the DoOR 2.0.1 dataset [70, 71], a comprehensive database of olfactory responses from various measurement techniques such as single sensillum recordings, calcium imaging, and heterologous expression [49, 72–92]. If the predicted OR structures are accurate, we expected that neuronal activity would correlate with the binding of the response-inducing molecule to the OR model. We initially focused on terpenes, a class of carbohydrates with a large natural abundance, because we speculated that these molecules were a feasible target for a computationally relatively simple molecular docking approach. We calculated the binding energy of terpenes, to the generated OR structures using Vina Dock (see Materials and Methods) for a subset of Dm ORs and plotted these against the measured neuronal response from the DoOR dataset (Figure 3, left). We found that the difference in binding energy between responding (> 0) and non-responding neurons (≤ 0) was highly significant (Student’s t-test, $p < 3 \cdot 10^{-7}$), suggesting that the predicted structures have realistic binding pockets for terpenes. Motivated by this, we investigated the same Dm OR

subset using all molecules present in the DoOR dataset. Here, we obtained a weak correlation between neuron activation and binding energy (Figure 3, right). At this point it is unclear whether the scatter can be explained by the uncertainty of the molecular docking method or point to more complex molecular recognition mechanisms. Currently, we are investigating an even larger number of ORs and binding molecules with refined computational approaches. If the responses of olfactory neurons to odors are indeed explained simply by the binding energy of an odor to the OR, the molecular recognition process of insect olfaction can be condensed into a measure of this binding energy. Taken together, these results show the potential to use computational tools to predict OR to odor response.

3.2. Surface stabilization of Orco-OR complexes in synthetic cells

To measure the binding of ORs to odor molecules, OR receptor proteins are typically immobilized on surfaces. To avoid stability problems associated with the immobilization of individual receptors [57], we based our system on previous approaches that immobilized lipid membrane vesicles on an electrode surface [42, 93]. Such vesicles not only provide a native lipid environment but are also able to maintain a membrane potential through ion asymmetry. As in biological sensory neurons, the vesicle membrane potential can be depolarized by Orco-OR channel opening upon ligand binding. In recent years, lipid vesicles with an increasing number of such life-like features are also referred to as synthetic cells and are a field of active developments [94]. The increasing number of available synthetic cell modules provides a promising basis to detect the odor to OR binding by event-driven ionic currents, as in biological neurons.

To address the challenge of the necessary co-design approach, we developed a quantitative model of the proposed assembly of lipid-membrane-stabilized Orco-OR ion channels on an electrode. In the model, a fixed number of ion channels generate a current that flows into the electrode impedance. The ion channel was modeled as a resistor with two conductance states, and the electrodes were considered as a parallel resistor-capacitor circuit. The cleft between the synthetic cell and the electrode acts as a resistive element and is relatively large due to the nanoscopic dimensions of the cleft (see Materials and Methods). Analysis of the model showed that the vesicle radius r is an important design parameter. The total charge in a synthetic cell scales with r^3 , while the number of ion channels scales with r^2 . Thus, we expect two regimes with different vesicle sizes: one regime dominated by the finite number of charges encapsulated in smaller vesicles, whereas signals from larger vesicles are sensitive to the densities of inserted ion channels. In addition, the overall coverage of signal-generating synthetic cells depends on the ratio of electrode size to vesicle size. In experiments, the sizes of vesicles are readily tuned between 100 nm and 100 μm , providing an opportunity to test the different regimes predicted by the model.

3.3. Selection methodology for odor receptors (OR) and synthetic dataset

We now discuss our procedure for selecting the odorant and OR sets, and how we model sensor responses. Our approach allows us to answer the following co-design questions:

- For a given set of odors we want to distinguish, which ORs need to be considered?
- What magnitude of response signal is expected for an individual synthetic cell?
- How many synthetic cells of the same receptor type are required for sufficient SNR, and which quality is required of the electrode and amplification stages?
- Which network models are suited to successfully discriminate sensor data?

To this end, we make use of a synthetic dataset based on measurements of odorant responses in *Drosophila melanogaster*. In the DoOR dataset, all recordings have been merged and normalized across studies, providing response data for 78 types of sensory units to 692 odorants. As we aim to reconstitute OR, we exclude units from the dataset which can not be clearly linked to a single OR type, such as responses from multiple receptor types or ionotropic receptors. This leaves our analysis with a total of 52 possible OR types.

We first need to restrict the number of ORs and odorants. The task is to find the minimal number of ORs we need to reconstitute in order to reliably differentiate between a given set of odors. This can be seen as a separation task in the space of responses of all receptors, see Figure 4 (left). We achieve this by calculating the ‘odor separability’, i.e. the Euclidean distance between the response vectors to the odor, and iteratively excluding the OR which contributes least to separability; see Section 5.4 for a detailed description of the method.

Our analysis yields the odor separability for different sets of odorants vs. the number of enabled ORs, as shown in Figure 4 (center). For illustration, we have chosen three sets of odors with differing degrees of relationship in terms of chemical structure (blue, orange, and green sets). As expected, all odor sets show better separability with larger number of different receptors; however, relative separability naturally depends on the combination of odors we are probing (note that results are normalized *across* odorant sets). Blue: three odorants from different functional groups (respectively: alcohols, esters, and lactones) show large relative separability. Orange: separability is reduced when considering less diverse functional groups (here: alcohols and aromatic alcohols). Green: odorants from a single functional group with similar OR responses are naturally less separable. Note that we control against the possibility of no ligand binding at all for a given odorant by including a ‘none’ odor; see Section 5.4 in Materials and Methods.

Most importantly, our algorithm tells us exactly which ORs need to be reconstituted for optimal separability of odors and subsequent discrimination of odors by our sensing platform. As an example, Figure 4 (right) shows the most relevant ORs for $N_{\text{OR}} = 3$ for the aforementioned odor sets.

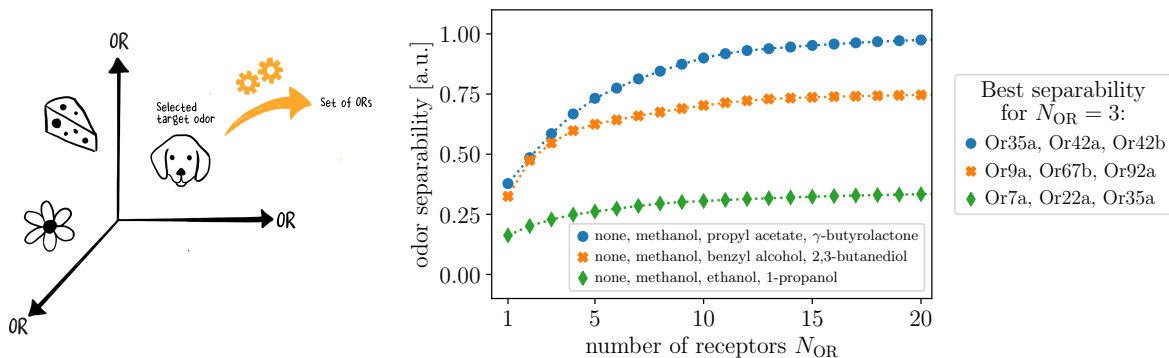


Figure 4: *Left*: OR/odor space, exemplified by three smells that occupy a space defined by the responses of different ORs. Our algorithm selects OR for maximum separability in the OR space. *Center*: Normalized odor separability vs. number of Dm ORs for different sets of odorants. *Right*: ORs showing highest separability for each odor set for $N_{OR} = 3$.

Having selected the odor/OR sets of interest, we now construct a synthetic dataset of sensor responses. To do so, we define a simple ion channel model for individual ORs, and subsequently combine their signals in an electrode response model derived from the parameters determined in Section 3.2.

For a single OR, the response to the binding of an odor molecule is modeled as a stochastic process with N_{ORCO} ion channels. If the ligand binds to a closed Orco channel, the channel opens, and current flows out of the vesicle until stochastic unbinding occurs. We thus define a Markov model with the opening probability of Orco p_{open} and closing with p_{close} . The open and closed states are converted to currents by comparison with the electrophysiological characterization of VUAA1-induced Orco currents; see Section 5.5 and Butterwick et al. 2018 [67], in particular Extended Data Fig. 2. Similarly, ion channel noise and low-pass filter properties of the vesicle membrane are modeled on the basis of electrophysiological characterization. To obtain the current flow of an OR of a single receptor type, we then sum over all of its Orco currents. For the electrode response, we assume that the electrode can probe individual ORs; thus, the sensor response to an odor molecule is given by a low-pass filter of the individual OR current, which we parametrize with the electrode model described in Section 3.2. From this procedure, we obtain a time series of voltages with sensor responses per odor–OR type combination, see Figure 5. The model is flexible with respect to which odorants and ORs to simulate, supporting the full DoOR 2.0.1 dataset of 692 odors and 52 OR types. In order to increase realism w.r.t. actual measurement conditions, the onset of odor presentation is chosen at random within the full simulation time window.

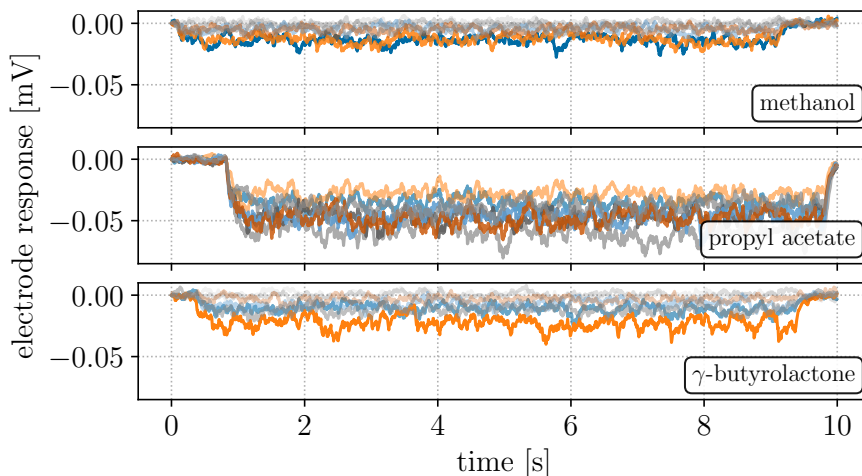


Figure 5: Simulated electrode responses to three odorants. Each trace shows the response of one synthetic cell comprising 10 Orco-OR complexes of the same receptor type; different receptor types are color-coded. We show the 7 most relevant OR types, as determined by our OR reduction algorithm. Opacity of traces is scaled with maximum voltage for better readability. Note that the odor is only presented during a portion of the overall time frame (presentation onset after 0.05 s, 0.8 s, 0.4 s, from top to bottom).

3.4. Odor discrimination with a spiking neural network model

The dataset presented above allows us to estimate the sensor responses for different sets of odorants. We now proceed further down our processing pipeline by modeling the neural network stage. To do so, we train a spiking neural network (SNN) to classify odors based on the electrode responses. The SNN architecture used for this task consists of three fully connected layers. The number of input neurons is determined by the number of different ORs used as the sensing front-end, while each output neuron corresponds to a specific odor class. The neurons in the model follow the Leaky-Integrate-and-Fire (LIF) model, with the subthreshold dynamics described by the following equation:

$$V_{mem,i}(t) = \alpha V_{mem,i}(t-1) + \sum_{j \neq i} w_{i,j} \sigma_j(t) + \frac{I_{dc}(t) \cdot \Delta t}{C} \quad (1)$$

where V_{mem} is the membrane potential of neuron i , j is the presynaptic neuron index, $\sigma(t)$ is the spike at time t from neuron i to j , α is the membrane decay factor, Δt is the time step and C is the membrane capacitor for charge accumulation and leakage. When the membrane potential reaches the threshold value V_{thr} the neuron emits one spike at time t .

Training is performed using backpropagation through time (BPTT), an algorithm that involves calculating derivatives across all layers and time steps. Since neuron spikes are discrete, we use a straight-through estimator based on a sigmoid function [95]. The SNN architecture provides advantages in processing efficiency during inference due to

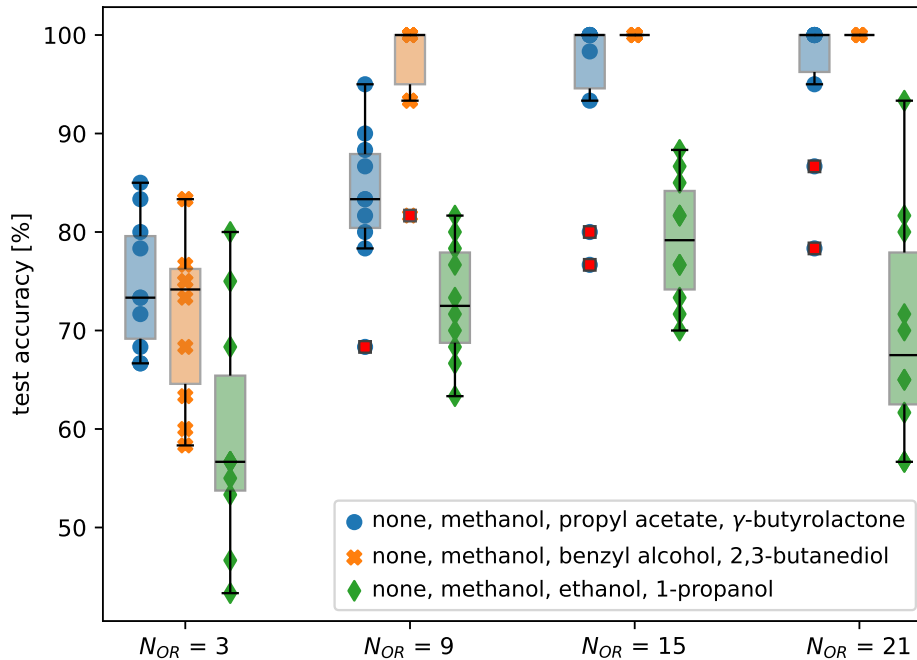


Figure 6: Test accuracy (median and quartiles) for classification of three different sets of odorants (outliers are marked in red squares), with varying numbers of receptors (3, 9, 15, and 21). The number of hidden layer neurons is fixed at 100. Training was performed 10 times for each set of odorants. All weights were quantized to 4 bits.

its massively parallel spiking behavior. Additionally, the implementability of the weight matrix is further optimized through quantization to four bits.

In this case study, the same odor sets (blue, orange, and green) used in the previous subsection were selected for classification (see Fig. 4). For each odorant, synthetic response traces were generated. The response values for each OR at each time step were organized into a response matrix, where the height of the matrix corresponds to the number of ORs and the width of the matrix represents the number of time steps. This time series was sequentially fed into the MLP SNN, column by column, with the analog value passed into the input-to-hidden linear layer, followed by an activation function which defines the behavior of membrane potential update. The following layer operates in the same manner. The spike outputs for each odor category were then summed across all time steps for each sample. The resulting test accuracy is shown in Fig. 6. As these results demonstrate, the SNN learns to classify the odor sets; however, as expected, the classification accuracy depends on the number of receptors and the chemical structure of the odors.

Note that the SNN classification results do not exactly follow the odor space analysis of Fig. 4; for example, the blue set is classified with lower accuracy, even though it has higher separability. We attribute this to our definition of separability of odors as the linear distance between odor responses. Therefore, a non-linear analysis like an SNN can

exploit deeper underlying correlations, skewing the classification results across odor sets. These SNN results can be seen as baseline results, with more complex and biorealistic networks and algorithms required to tackle continual learning, drift compensation, and more complex odor combinations (see Discussion).

3.5. Electronic sensing pad and neuromorphic hardware implementation of the spiking neural network model

An illustration of the complete hardware architecture is shown in Fig. 7. The proposed system consists of an analog front-end designed to process chemosensory signals using an event-driven analog spiking neural network architecture. By bypassing analog-to-digital converters (ADCs) and by leveraging novel synthetic biological assemblies, this approach enables real-time, low-power operation suitable for always-on applications. The system is manufactured in the SkyWater 130 nm CMOS process and integrates: i) a bioelectro interface that couples lipid vesicles with synthetic olfactory receptors (OR) and microelectrode arrays, and ii) a low-noise analog amplifier for signal conditioning. iii) a neuromorphic spiking neural network that processes sensor responses in a low-power mixed-signal domain.

The design exploits transistors operating in the weak inversion (subthreshold) regime. This ensures that tunable device parameters (e.g., bias voltages and currents) can be directly mapped to the computational model, thereby aligning hardware behavior with algorithmic specifications. The range and granularity of these tunable parameters are influenced by physical circuit constraints, including transistor dimensions and the overall network topology. Comparisons between the algorithmically specified neurons and their hardware realizations are critical in verifying the implementation of the design. Therefore, in this section, we simulate the neuron and synapse circuits independently to evaluate their functional behaviors, focusing on how supply and bias voltages affect circuit operation.

Specifically, we provide simulation results of the neuron and synapse circuits separately and analyze their behavior, including voltage dependencies.

The schematic overview of the neuron circuit is shown in Fig. 7 “NEURON” block. Three node voltages (V_{dc} , V_{leak} , and V_{ref}) are used to control the membrane potential V_{mem} , that is, the voltage across the capacitor C_1 , influencing its charging speed, discharging speed, and refractory period, respectively. The behavior of V_{mem} below the firing threshold is described by equation 1, in which the voltage at the node V_{leak} corresponds to the decay of α , and V_{dc} controls a constant injection of current (I_{dc} in equation 1). Due to this constant charging behavior, the model parameter α depends on V_{mem} and is expressed as:

$$\alpha = 1 - \frac{R_{leak} \cdot \Delta t}{V_{mem}} \quad (2)$$

where R_{leak} is the leakage rate (V/s), and Δt is the chosen time step.

The neuron operates asynchronously, which means it generates signals (or pulses) at unpredictable intervals rather than at fixed, regular intervals. To reliably inform

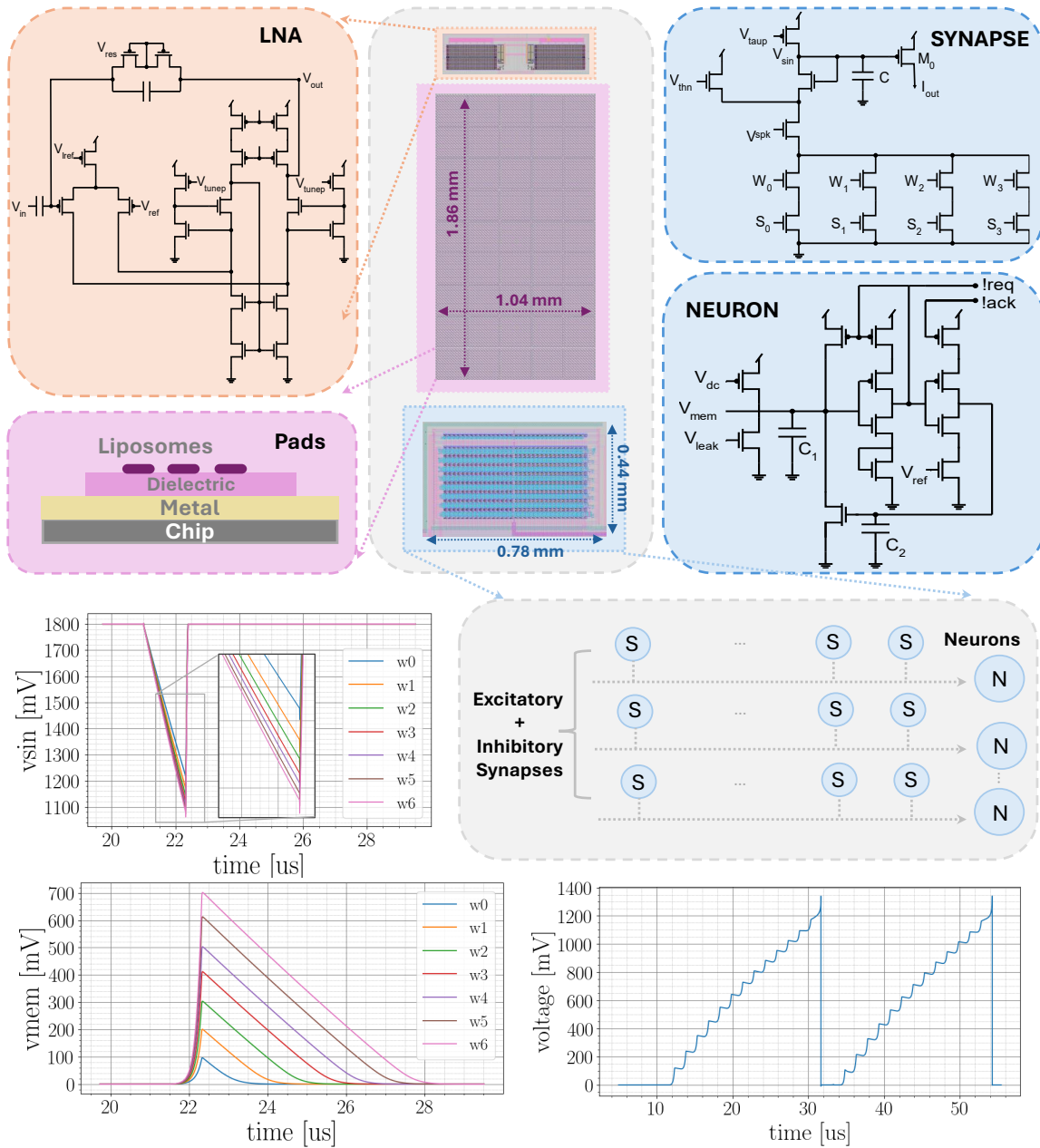


Figure 7: Overview of the hardware implementation, including the layout and schematic view of individual blocks. The components are as follows: Low Noise Amplifier (LNA) (upper left), pads for the sensing front-end (upper left), and the neuron tile with synapses (upper and center right). The Ngspice simulation results are shown below: voltage update at node V_{sin} (center left), membrane potential across the capacitor C_1 in the NEURON block updates for an equivalent three-bit resolution ranging from 100 mV to 700 mV in seven equal intervals named $w_0, ..w_6$ (bottom left), and membrane potential integration with low leakage (bottom right). The physical analog circuits support 4-bit analog weights ($W_{0,1,2,3}$), and results in seven distinguishable weight values ($w_0, ..w_6$).

a receiving system, such as a microcontroller, whenever a pulse occurs, we use a 4-phase handshake protocol involving two signals: *!req* (request) and *!ack* (acknowledge). When the neuron generates a pulse, it raises the *!req* signal to notify the receiver. The receiver then acknowledges this by raising the *!ack* signal. Upon receiving this acknowledgment, the neuron retracts its request (*!req*), confirming that the pulse has been successfully transmitted. Finally, the receiver lowers its acknowledgment (*!ack*), completing the handshake cycle. This process ensures accurate and reliable communication of asynchronous pulse events between the neuron and microcontroller.

The neuron receives input from the preceding layers of neurons through the synapse circuit, whose schematic is shown in Fig. 7 “SYNAPSE” block. The variables $W[0 \sim 3]$ define the weight (current) for each bit, while $S[0 \sim 3]$ act as switches to enable their respective contributions. The output current, i_{out} , represents the weighted spike contribution and is directly injected into V_{mem} of the neuron circuit. The resulting charging behavior of V_{mem} is illustrated in Fig. 7 (bottom). To balance the parameters between bias and weight matrix, the transistor sizes for the input dc and the weighted spike are deliberately designed to be different.

The relationship between $V_{W[0\sim3]}$ and the discharge rate $R_{V_{sin}}$ of the node V_{sin} follows a simple subthreshold MOS transistor transfer characteristic, of which the equation is 3.

$$R_{V_{sin}} = \frac{dV_{sin}}{dt} = \frac{I_{tot}}{C} = \frac{1}{C} \sum_{Branch\ i} \frac{I_{ds,0_i} W_i}{L_i} e^{\frac{V_{W_i} - V_{th,n}}{nU_T}} \quad (3)$$

Where V_{th} is the transistor threshold voltage, $U_T = \frac{KT}{q}$ and can be approximated to $25mV$ under $300K$ and $n = 1 + \frac{C_D}{C_{ox}}$ with C_{ox} being oxide capacitance, and C_D representing depletion capacitance.

Subsequently, the node V_{sin} is converted to a current i_{out} by a P-type MOSFET M_0 . Ultimately, i_{out} charges the V_{mem} of the neuron. This contribution corresponds to the second term, $\sum_{j \neq i} w_{i,j} \sigma_j(t)$, in Equation 1. It is important to note that the exponential characteristic of M_0 complicates the precise representation of the bit value.

3.6. Hybrid synthetic sensory neuron

We simulated the full signal processing pipeline from the ion dynamics on the microelectrode to the firing of VLSI spiking neurons. The microelectrode pad array is responsible for detecting low-amplitude bioelectronic signals in the tens of microvolt range (as shown in Fig. 8 top), which are then fed into a low-noise amplifier (LNA) for signal conditioning. The LNA enhances weak signals, providing an output swing of approximately 5-10 mV with a gain of 50.05 dB, ensuring reliable signal amplification while preserving fidelity (second plot in Fig. 8). This amplified signal is then processed by spiking neurons, where the modulated activity of current injection is provided by connecting the LNA output, after scaling, to the (V_{dc}) nodes, directly stimulating somatic circuits to generate spikes. The event-driven nature of this architecture enables efficient signal encoding, where spike generation is proportional to the detected signal strength, facilitating mean rate coding for robust event-based detection (three bottom plots in Figure 8). A comprehensive simulation captures the entire signal processing pipeline, where soma circuits are maintained near the threshold by balancing the contributions of injection and leakage currents (V_{dc} and V_{leak}), allowing neurons to rapidly generate spikes upon detection of simulated odor signals on the pad.

By integrating synthetic biological components with VLSI circuits in this manner, a new class of neuron emerges, the *hybrid synthetic sensory neuron*, wherein the hybrid interface from pad to amplifier to soma enables event-driven detection and spike generation.

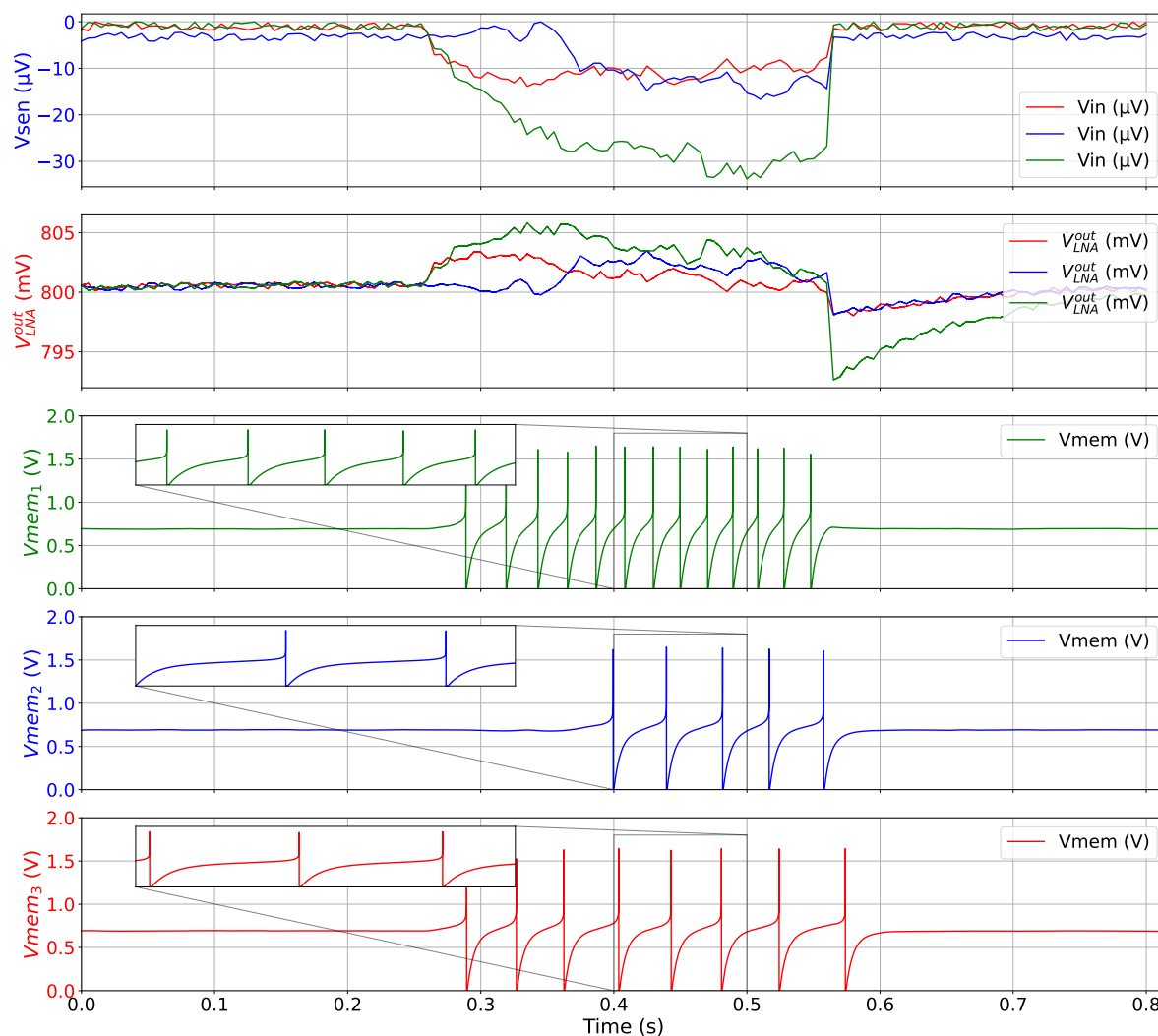


Figure 8: Ngspice simulation results for a hybrid synthetic sensory neuron for analog-to-spike coding: The top plot illustrates three input traces derived from the synthetic dataset, which are applied to the LNA’s input. The second plot displays the LNA’s voltage output, demonstrating an output swing of approximately 100 mV with a gain of 50.05 dB. This amplified output is then utilized to modulate three current injection nodes (V_{dc}), which directly stimulate the somatic circuits, triggering neuronal firing as shown in the last three plots.

4. Conclusions & Outlook

This work presents a novel co-design methodology and a neuromorphic chemosensing system that aims at integrating biological olfactory receptors with analog neuromorphic circuits, mimicking natural olfactory processing. By combining biological odor receptors with neuromorphic hardware, we aim to achieve real-time, energy-efficient chemosensory detection. The use of weak-inversion transistors and event-driven spiking neural networks ensures on-demand processing, minimizing power consumption while maintaining high sensitivity to chemical stimuli.

As we have outlined, our approach is unique in that it combines the physical realization of sensory neurons, processing, and learning mechanisms, all in one device. To reach this goal, we build on recent advances in the use of machine learning methods in biology to enable the co-design with the established electrical engineering methods.

A key component is the bioelectronic interface, which bridges biological odor recognition with CMOS-based electronics. To enhance signal transduction, it will be necessary to characterize the synthetic cell-electrode interface and to optimize the electrode impedance for improved sensitivity and signal integrity.

While process variations and mismatch in weak-inversion circuits may introduce variability, the system integrates multiple biasing mechanisms to compensate for these effects, which will be further validated during hardware testing. The bigger source of drift and variability might stem from the biological receptors, for example by leakage of ions from the synthetic cell vesicles. This will make it necessary to adapt electrical methods for compensation, e.g. DC drift offset compensation, or more systematic approaches like homeostatic learning mechanisms.

We plan to extend the current work with hardware characterization, comprehensive dataset collection, and system scalability. Specifically, efforts will be directed toward expanding the platform to support multiple sensor pads, each featuring distinct odor receptor chambers, thereby enhancing the system’s capability to distinguish between a wider range of chemical compounds. In addition, spiking neural network classifiers will be used to achieve real-time classification of complex odor mixtures, paving the way for practical applications in autonomous chemical analysis.

The results of our model pipeline give us strong guardrails for the development of our platform, informing the co-design of Orco-OR complexes, vesicle properties, amplification stages, and decoding hardware. As seen in Fig. 6, the classification of the odor is confounded by the noise and the number / types of available OR. In this regard, we interpret the SNN classification results as a baseline.

In addition, as part of our co-design, we are developing network models which are able to extract relevant information delivered from the sensors, such that high classification accuracy with minimal number of ORs can be achieved. A crucial data feature may be the temporal structure of the stimulus. The hardware simulations shown here are based on the direct injection of the sensor current into the first layer of neurons, effectively resulting in rate coding with a bin width of $\mathcal{O}(200)$ ms (Fig. 8). By

adapting circuit components, we are able to change the time constants to fully exploit the temporal structure of the stimulus. Alternatively, coding schemes such as precise spike timing have been observed in our model species [96], and may prove valuable for our application.

The setup described here is limited to supervised training using single odorants. Future work will investigate odor mixtures as they appear in real-world applications. Due to OR co-activation, it is unclear which response to expect from the synthetic cells, and careful characterization of the odor mixtures will be needed. Finally, we aim to investigate unsupervised and few-shot learning for real-world use of our sensing platform.

5. Materials & Methods

5.1. Orco-OR complex stability

Odor receptor amino acid sequences were obtained from UniProt [92], with the search query '(protein_name:"odorant receptor") AND (taxonomy_id:XXXX)'. Species associated with olfactory research were selected (see Supplementary Material for used taxonomy ids). The list was manually cleaned for duplicates and fragment sequences. The total of 348 sequences were assembled into 1:1 complexes with the *Drosophila melanogaster* Orco channel (Uniprot id Q9VNB5) using Alphapull-down scripts [93]. Complex structures were predicted using AlphaFold v2.3.1. In addition to generation of .pdb files that were further analyzed with Chimera (ChimeraX 1.9), the script produced a list of the complexes with different scoring metrics. Two of the scores were used to filter for accurate and stable complexes. The dataset (252 insect species, 48 *Dm* and 48 *M. musculus* complexes with *Dm* Orco) was first sorted using the ipTM score applying a cut-off of 0.6. The ipTM score is derived from pairwise distance error predictions for interface residues [64, 65]. For complexes above ipTM > 0.6 the interface solvation energy was calculated from the residues contributing to the protein-protein interface [66].

5.2. Molecular Docking

AlphaFold (version 2022-11-01) structures of olfactory receptors were obtained from Uniprot. Potential binding sites were identified using P2Rank [97]. Terpenes were represented using their respective SMILES strings. The SMILES structures were converted into 3D coordinates using RDKit (version 2024.9.5). Docking was performed using AutoDock Vina [98] with an exhaustiveness parameter set to 32. The search space was defined based on the P2Rank-predicted binding pocket coordinates in a box of $5 \times 5 \times 10$ Å. The binding energy of the most favorable pose was reported.

5.3. Electrode model

Multielectrode Arrays (MEAs) consisting of 60 titanium nitride electrodes of 30 μm diameter (Model 60tMEA200/30iR-ITO-gr, Multichannel Systems, Germany) were characterized using impedance spectroscopy. Impedance spectra in the frequency range 10 kHz to 1 MHz were obtained in phosphate buffer solution of physiological salinity at room temperature. A three-circuit model consisting of a resistor in series with capacitance (C_{dl}) and a resistor (R_t) in parallel was used to fit the spectra with $\chi^2 \approx 0.2$. The resistance of the gap R_{gap} was calculated from $R_{gap} = \rho_s / (5\pi d_{gap})$, with approximate values for the solution of conductivity $\rho_s = 1 \text{ } \Omega\text{m}$ and $d_{gap} = 1 \text{ nm}$ [93, 99]. The final values for the electrode model are $R_{gap} = 6.37 \times 10^7 \text{ } \Omega$, $C_{dl} = 8.99 \times 10^{-11} \text{ F}$, and $R_t = 7.92 \times 10^8 \text{ } \Omega$.

5.4. Odor space analysis

We describe our method for selecting the most viable ORs for a given set of odorants in Algorithm 1. The method requires a response data matrix with entries (odor \times OR), which we have retrieved from the DoOR 2.0.1 database [70, 71]; specifically, we use the provided `door_response_matrix.csv`, which contains responses of 78 sensory unit types to 692 odorants, normalized to $[0, 1]$ across all responding units. We first exclude all unit types not clearly linked to a single OR type, as described in [71], which leaves a total of 52 ORs to be analyzed. As only a subset of all unit type/odor combinations have been measured (about 14%), we replace missing entries (NA) with zero response. This may introduce the issue that some odors are separated only by the absence of any response; in practice, this would make it impossible to distinguish such an odor from noise currents when no ligand is present. We mitigate this issue by including a ‘no ligand/none’ odor in the analysis, see below.

From the response data, we select only the odorants (rows) in which we are interested. Our method then iteratively removes ORs (columns) from the response matrix, until the desired number N_{OR} of ORs to be reconstituted is reached. The OR to be removed is selected by the criterion of ‘odor separability’, which is the sum of all Euclidean distances of rows (odorants). This means that we exclude one OR from the data, and compare the response of the remaining ORs to the odors. The higher the Euclidean distance, the higher the odor separability. We find the least important OR by comparing the separabilities with that OR excluded: If we denote as $D_{\setminus j}$ the responses of all ORs minus receptor j , then that $D_{\setminus j}$ which has the highest separability is the one we want to continue with. We thus pick the receptor j for which the separability of $D_{\setminus j}$ is reduced the least, and eliminate it from the pool of receptors. This procedure is repeated iteratively until the desired number N_{OR} is reached.

Our algorithm for selecting odor/OR sets is easily implemented and performs the reduction quickly. Note however that the underlying dataset corresponds to response measurements of olfactory receptor neurons corrected for the baseline firing rate, and doesn’t cover cases where no ligand is present at all, as described above. Therefore, if

the final selection given by our algorithm includes odors for which none of the selected ORs respond at all, this odor will be experimentally indistinguishable from no ligand binding. To cover this case, we have included a ‘no ligand/none’ odor, i.e. a row in D_{all} which has zero response for all OR.

Algorithm 1 OR reduction algorithm

Require: desired number of ORs N_{OR} , indices of desired odorants $\{i\}$, response data D_{all} with entries (odor \times OR)

```

 $N \leftarrow N_{\text{OR}}^{\text{total}}$                                 ▷ total number of columns in dataset  $D_{\text{all}}$ 
 $D \leftarrow D_{\text{all}}[\{\text{rows } i\}]$                     ▷ only take odorants we are interested in

while  $n > N_{\text{OR}}$  do                                ▷ until desired number of ORs is reached
  for  $j$  in columns of  $D$  do                            ▷ for each OR  $j$ 
     $D_{\setminus j} \leftarrow D[\{\text{columns } \neq j\}]$         ▷ exclude OR  $j$  responses
     $S(D_{\setminus j}) \leftarrow \sum_{m \neq n} \| \text{row } m \text{ of } D_{\setminus j} - \text{row } n \text{ of } D_{\setminus j} \|$   ▷ calc. odor separability
  end for
   $j_{\text{elim}} \leftarrow \text{argmax}_j [S(D_{\setminus j})]$             ▷ select OR for which highest separ. remains
   $D \leftarrow D[\{\text{columns } \neq j_{\text{elim}}\}]$           ▷ eliminate that OR
   $n \leftarrow n - 1$ 
end while

```

5.5. Synthetic dataset

The synthetic dataset is modeled using a Markov model of Orco ion channels. We assume that each synthetic cell only has one specific OR type, and that there are N_{ORCO} ion channels per synthetic cell in proximity to each electrode. In order to model Orco realistically, we compare our simulation with the electrophysiological characterization of VUAA1-induced Orco currents, matching the data of Extended Data Fig. 2 in Butterwick et al. 2018 [67].

To generate a voltage trace of one Orco for a given odor/OR type combination, we perform the following steps:

- (i) fetch the normalized odor/OR response $d_{\text{odor,OR}}$ from the response dataset D .
- (ii) simulate a two-state Markov model with channel opening and closing probabilities p_{open} and p_{close} for $(T_{\text{data}} \times dt)$ steps (‘data trace’). The channel opening probability is given by $p_{\text{open}} = p_{\text{close}} \times d_{\text{odor,OR}}$.
- (iii) convert the open and closed states to currents in pA by drawing from $\mathcal{N}(\mu_{\text{open}}, \sigma_{\text{open}})$ and $\mathcal{N}(\mu_{\text{closed}}, \sigma_{\text{closed}})$, respectively.
- (iv) generate ion channel noise for $(T_{\text{total}} \times dt)$ steps and filter to match the noise found in [67]. To match the magnitude and frequency spectrum, we compare to the parts of the recording where no ligand is present.

(v) randomly shift the data trace in time and add to the noise trace.

For each synthetic cell, we perform these steps N_{ORCO} times and sum the current traces. Finally, we obtain the voltage induced in the electrode by modeling an RC circuit which integrates the generated current. The parameters R_{gap} , C_{dl} and R_t are determined from impedance spectroscopy (see Section 5.3). The transition probabilities $\{p_{\text{open}}, p_{\text{close}}\}$ of the Markov model were estimated based on Orco measurements from Ref. [67]. In particular, these recordings show baseline noise $\mathcal{O}(0.5 \text{ pA})$, some signal currents of about 2 pA, and larger portions of signal showing current flow of 2 to 5 pA. The former can be attributed to a single Orco opening, while the latter is potentially caused by multiple Orcos being probed at the same time. In order to make a conservative estimate of a single Orco current, we base the Markov model parameters only on a portion of the signal which contains current flow up to 2 pA (central region in Extended Data Fig. 2c of [67], corresponding to the range from 48.9 s to 49.6 s in the recordings provided by the authors). Similarly, the parameters $\{\mu_{\text{open}}, \sigma_{\text{open}}\}$ and $\{\mu_{\text{closed}}, \sigma_{\text{closed}}\}$ have been chosen to match the binned data generated from the same region of measurement.

For all parameters and implementation details, see the code repository [100].

5.6. Design and Simulation of the Neuromorphic Hardware Platform

The system integrates an analog front-end with an event-driven, asynchronous spiking neural network and a microcontroller. It consists of: (i) a bioelectronic interface coupling lipid vesicles with synthetic olfactory receptors and microelectrode arrays, (ii) a low-noise analog amplifier for signal conditioning, (iii) a spiking neural network for energy-efficient sensor response processing, and (iv) a RISC-V microcontroller for spike decoding and synaptic weight configuration. Figure 9 illustrates the layout of the full chip. The low-noise amplifier (LNA) exploits a folded cascode OTA (FC-OTA) with an active cascode and a flipped current follower (FCF) to improve signal integrity, transconductance efficiency, and noise performance. The FC-OTA topology enhances gain while maintaining a wide output swing, the active cascode increases output impedance for better gain stability, and the FCF reduces impedance at the folded node, ensuring efficient current transfer. A detailed overview of these techniques is provided, with further details in the work by R. Sanjay et al. [101]. Somatic and synaptic circuits are designed with weak-inversion transistors and follow the principles of well-known neuromorphic designs [102, 103] that have been demonstrated to scale to advanced technologies nodes [104, 105].

The simulation results of the hardware platform are obtained using Ngspice. The complete hardware system is currently being manufactured by Efabless and shown in Figures 7 and 9, where we provide a detailed overview of the device, illustrating the four key components and the chip layout. The reference pad serves as a stable biasing point for the chip, allowing the analog front-end and neural processing circuits to operate with respect to a well-defined potential. This is especially important for minimizing common-mode noise and ensuring reliable signal transduction from the bioelectronic

interface. The spiking neural network includes a total of 16 neurons and 512 synapses, organized to support configurable connectivity patterns. This configuration enables efficient encoding of sensory inputs and supports spike-driven odor classification.

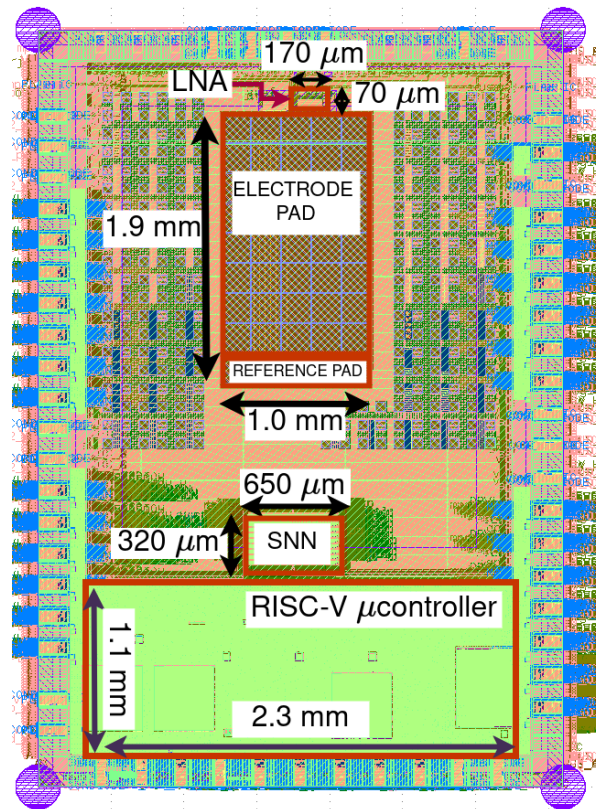


Figure 9: The full chip layout in SkyWater 130 nm features an electrode pad interface (1.6×1.0 mm), a reference pad (0.2×1.0 mm), low-noise amplifier ($170 \times 70 \mu\text{m}$), a mixed-signal spiking neural network (SNN) processor ($650 \times 320 \mu\text{m}$), and a 32-bit RISC-V (RISCV32IMC) μ controller (1.1×2.3 mm).

Acknowledgments

This work is part of the project *SYNCH: Combining SYnthetic Biology & Neuromorphic Computing for CHEmosensory perception*, funded by the Volkswagen Foundation under the call “NEXT — Neuromorphic Computing”. We gratefully acknowledge the foundation’s initiative to unite diverse disciplines in the pursuit of novel scientific ideas and their continued support in making this research possible. We also thank Josefina del Marmol for providing recorded data characterizing Orco and helpful explanations.

References

- [1] Wenxing Yang, Taihong Wu, Shasha Tu, Yuang Qin, Chengchen Shen, Jiangyun Li, Myung-Kyu Choi, Fengyun Duan, and Yun Zhang. Redundant neural circuits

- regulate olfactory integration. *PLoS Genetics*, 18(1):e1010029, 2022.
- [2] Magda Brattoli, Gianluigi De Gennaro, Valentina De Pinto, Annamaria Demarinis Loiotile, Sara Lovascio, and Michele Penza. Odour detection methods: Olfactometry and chemical sensors. *Sensors*, 11:5290–5322, 2011.
- [3] Jordi Fonollosa, Agustin Gutierrez-Galvez, and Santiago Marco. Quality coding by neural populations in the early olfactory pathway: analysis using information theory and lessons for artificial olfactory systems. *PloS one*, 7(6):e37809, 2012.
- [4] Baranidharan Raman et al. Mimicking biological design and computing principles in artificial olfaction. *ACS chemical neuroscience*, 2(9):487–499, 2011.
- [5] Tomasz Wasilewski, Nathália F Brito, Bartosz Szulczyński, Marek Wojciechowski, Natalia Buda, Ana Claudia A Melo, Wojciech Kamysz, and Jacek Gębicki. Olfactory receptor-based biosensors as potential future tools in medical diagnosis. *TrAC Trends in Analytical Chemistry*, 150:116599, 2022.
- [6] Poonam Prasad, Piyush Raut, Sangita Goel, Rajesh P Barnwal, and GL Bodhe. Electronic nose and wireless sensor network for environmental monitoring application in pulp and paper industry: a review. *Environmental Monitoring and Assessment*, 194(12):855, 2022.
- [7] Álvaro Rocha et al. *Europe and MENA cooperation advances in information and communication technologies*. Springer, 2017.
- [8] Manhougbé Probus Aymard Farel Kiki, Sèmèvo Arnaud Roland Martial Ahouandjinou, Kokou Marc Assogba, and Tole Sutikno. Bibliometric analysis and survey on electronic nose used in agriculture. *International Journal of Electrical & Computer Engineering (2088-8708)*, 14(2), 2024.
- [9] Theerapat Pobkrut et al. Sensor drone for aerial odor mapping for agriculture and security services. In *2016 13th International Conference on Electrical Engineering/Electronics, Computer, Telecommunications and Information Technology (ECTI-CON)*, pages 1–5. IEEE, 2016.
- [10] Sofie Bosch, Renée X de Menezes, Suzanne Pees, Dion J Wintjens, Margien Seinen, Gerd Bouma, Johan Kuyvenhoven, Pieter CF Stokkers, Tim GJ de Meij, and Nanne KH de Boer. Electronic nose sensor drift affects diagnostic reliability and accuracy of disease-specific algorithms. *Sensors*, 22(23):9246, 2022.
- [11] Tran Thi Dung, Yunkwang Oh, Seon-Jin Choi, Il-Doo Kim, Min-Kyu Oh, and Moonil Kim. Applications and advances in bioelectronic noses for odour sensing. *Sensors*, 18(1):103, 2018. Number: 1 Publisher: Multidisciplinary Digital Publishing Institute.
- [12] Abdelaziz Rabehi, Hicham Helal, Dario Zappa, and Elisabetta Comini. Advancements and prospects of electronic nose in various applications: A comprehensive review. *Applied Sciences*, 14(11):4506, 2024.
- [13] Taejung Kim, Yonggi Kim, Wootae Cho, Jong-Hyun Kwak, Jeonghoon Cho, Youjang Pyeon, Jae Joon Kim, and Heungjoo Shin. Ultralow-power single-sensor-

- based e-nose system powered by duty cycling and deep learning for real-time gas identification. *ACS sensors*, 9(7):3557–3572, 2024.
- [14] Sang Woo Lee, Byeong Hee Kim, and Young Ho Seo. Olfactory system-inspired electronic nose system using numerous low-cost homogenous and heterogeneous sensors. *Plos one*, 18(12):e0295703, 2023.
- [15] Bartosz Szulczyński et al. Determination of odour interactions in gaseous mixtures using electronic nose methods with artificial neural networks. *Sensors*, 18(2):519, 2018.
- [16] Nabil Imam and Thomas A Cleland. Rapid online learning and robust recall in a neuromorphic olfactory circuit. *Nature Machine Intelligence*, 2(3):181–191, 2020.
- [17] Caroline Bushdid, Marcelo O Magnasco, Leslie B Vosshall, and Andreas Keller. Humans can discriminate more than 1 trillion olfactory stimuli. *Science*, 343(6177):1370–1372, 2014.
- [18] Richard C Gerkin and Jason B Castro. The number of olfactory stimuli that humans can discriminate is still unknown. *eLife*, 4:e08127, jul 2015.
- [19] Thomas A Cleland, Szu-Yu T Chen, Katarzyna W Hozer, Hope N Ukatu, Kevin J Wong, and Fangfei Zheng. Sequential mechanisms underlying concentration invariance in biological olfaction. *Frontiers in neuroengineering*, 4:21, 2012.
- [20] Lu Xu, Dong-Jing Zou, and Stuart Firestein. Odor mixtures: A chord with silent notes. *Frontiers in Ecology and Evolution*, 11:1135486, 2023.
- [21] Xiao Liu, Sitian Cheng, Hong Liu, Sha Hu, Daqiang Zhang, and Huansheng Ning. A survey on gas sensing technology. *Sensors*, 12(7):9635–9665, 2012.
- [22] Baranidharan Raman, Joshua L Hertz, Kurt D Benkstein, and Steve Semancik. Bioinspired methodology for artificial olfaction. *Analytical chemistry*, 80(22):8364–8371, 2008.
- [23] Thomas Jacob Koickal et al. Analog vlsi circuit implementation of an adaptive neuromorphic olfaction chip. *IEEE Transactions on Circuits and Systems I: Regular Papers*, 54(1):60–73, 2007.
- [24] JA Covington et al. Towards a truly biomimetic olfactory microsystem: an artificial olfactory mucosa. *IET nanobiotechnology*, 1(2):15–21, 2007.
- [25] Mara Bernabei et al. Large-scale chemical sensor array testing biological olfaction concepts. *IEEE sensors journal*, 12(11):3174–3183, 2012.
- [26] Kea-Tiong Tang et al. Development of a portable electronic nose system for the detection and classification of fruity odors. *Sensors*, 10(10):9179–9193, 2010.
- [27] Michael Schmuker, Martin Nawrot, and Elisabetta Chicca. *Neuromorphic Sensors, Olfaction*, pages 2334–2340. Springer New York, New York, NY, 2022.
- [28] Nik Dennler, André van Schaik, and Michael Schmuker. Limitations in odour recognition and generalization in a neuromorphic olfactory circuit. *Nature Machine Intelligence*, 6(12):1451–1453, Dec 2024.

- [29] Alexander Vergara et al. Chemical gas sensor drift compensation using classifier ensembles. *Sensors and Actuators B: Chemical*, 166-167:320–329, 2012.
- [30] Xiaofang Pan, Jiebin Chen, Xiaolin Wen, Jiacheng Hao, Wei Xu, Wenbin Ye, and Xiaojin Zhao. A comprehensive gas recognition algorithm with label-free drift compensation based on domain adversarial network. *Sensors and Actuators B: Chemical*, 387:133709, 2023.
- [31] Abdunnasser Nabil Abdullah, Kamarulzaman Kamarudin, Latifah Munirah Kamarudin, Abdul Hamid Adom, Syed Muhammad Mamduh, Zaffry Hadi Mohd Juffry, and Victor Hernandez Bennetts. Correction model for metal oxide sensor drift caused by ambient temperature and humidity. *Sensors*, 22(9):3301, 2022.
- [32] Anup Vanarse, Adam Osseiran, and Alexander Rassau. An investigation into spike-based neuromorphic approaches for artificial olfactory systems. *Sensors*, 17(11):2591, 2017.
- [33] Ayon Borthakur and Thomas A Cleland. A spike time-dependent online learning algorithm derived from biological olfaction, *front. neurosci.* 13 (2019), 2019.
- [34] Shavika Rastogi, Nik Dennler, Michael Schmucker, and André van Schaik. The neuromorphic analog electronic nose. *arXiv preprint arXiv:2410.16677*, 2024.
- [35] C Virumbrales, R Hernández-Ruiz, M Trigo-López, S Vallejos, and JM García. Sensory polymers: Trends, challenges, and prospects ahead. *Sensors*, 24:3852, 2024.
- [36] Marielle El Kazzy, Jonathan S Weerakkody, Charlotte Hurot, Raphaël Mathey, Arnaud Buhot, Natale Scaramozzino, and Yanxia Hou. An overview of artificial olfaction systems with a focus on surface plasmon resonance for the analysis of volatile organic compounds. *Biosensors*, 11(8):244, 2021.
- [37] Richard Glatz and Kelly Bailey-Hill. Mimicking nature’s noses: From receptor deorphaning to olfactory biosensing. *Progress in neurobiology*, 93(2):270–296, 2011.
- [38] Yanli Lu and Qingjun Liu. Insect olfactory system inspired biosensors for odorant detection. *Sensors & Diagnostics*, 2022.
- [39] Yusuke Hirata et al. Biohybrid sensor for odor detection. *Lab on a Chip*, 21(14):2643–2657, 2021.
- [40] Jamal Ahmed Cheema et al. Insect odorant receptor-based biosensors: Current status and prospects. *Biotechnology Advances*, 53:107840, 2021.
- [41] Roshan Khadka et al. An ultrasensitive electrochemical impedance-based biosensor using insect odorant receptors to detect odorants. *Biosensors and Bioelectronics*, 126:207–213, 2019.
- [42] Tetsuya Yamada et al. Highly sensitive voc detectors using insect olfactory receptors reconstituted into lipid bilayers. *Science advances*, 7(3):eabd2013, 2021.

- [43] Santiago Marco et al. Signal and data processing for machine olfaction and chemical sensing: A review. *IEEE Sensors Journal*, 12(11):3189–3214, 2012.
- [44] Krishna C Persaud et al. Engineering aspects of olfaction. *Neuromorphic olfaction*, pages 1–58, 2013.
- [45] Mehmet K Muezzinoglu et al. Chemosensor-driven artificial antennal lobe transient dynamics enable fast recognition and working memory. *Neural computation*, 21(4):1018–1037, 2009.
- [46] Laurent Rattou et al. A comparative study of signal processing techniques for clustering microsensor data (a first step towards an artificial nose). *Sensors and Actuators B: Chemical*, 41(1):105–120, 1997.
- [47] Thomas Nowotny, Marien De Bruyne, Amalia Z Berna, Coral G Warr, and Stephen C Trowell. Drosophila olfactory receptors as classifiers for volatiles from disparate real world applications. *Bioinspiration & Biomimetics*, 9(4):046007, 2014.
- [48] Michael Schmuker et al. A neuromorphic network for generic multivariate data classification. *Proceedings of the National Academy of Sciences*, 111(6):2081–2086, 2014.
- [49] Michael Schmuker, Marien de Bruyne, Melanie Hähnel, and Gisbert Schneider. Predicting olfactory receptor neuron responses from odorant structure. *Chemistry Central Journal*, 1(1):11, 2007.
- [50] Timothy C Pearce et al. Rapid processing of chemosensor transients in a neuromorphic implementation of the insect macroglomerular complex. *Frontiers in Neuroscience*, 7:119, 2013.
- [51] Rinaldo Betkiewicz, Benjamin Lindner, and Martin P. Nawrot. Circuit and cellular mechanisms facilitate the transformation from dense to sparse coding in the insect olfactory system. *eNeuro*, 7(2), 2020.
- [52] Anna-Maria Jürgensen, Afshin Khalili, Elisabetta Chicca, Giacomo Indiveri, and Martin Paul Nawrot. A neuromorphic model of olfactory processing and sparse coding in the drosophila larva brain. *Neuromorphic Computing and Engineering*, 1(2):024008, 2021.
- [53] Chang Zhao et al. Predictive olfactory learning in drosophila. *Scientific Reports*, 11(1):6795, 2021.
- [54] Yang Shen, Sanjoy Dasgupta, and Saket Navlakha. Reducing catastrophic forgetting with associative learning: A lesson from fruit flies. *Neural Computation*, 35(11):1797–1819, 10 2023.
- [55] Thomas Pfeil and Others. Six networks on a universal neuromorphic computing substrate. *Frontiers in Neuroscience*, 7, 2013.
- [56] T.J. Koickal, A. Hamilton, T.C. Pearce, S.L. Tan, J.A. Covington, and J.W. Gardner. Analog VLSI design of an adaptive neuromorphic chip for olfactory

- systems. In *2006 IEEE International Symposium on Circuits and Systems*, pages 4 pp.–4550, 2006. ISSN: 2158-1525.
- [57] Charlotte Hurot, Natale Scaramozzino, Arnaud Buhot, and Yanxia Hou. Bio-inspired strategies for improving the selectivity and sensitivity of artificial noses: A review. *Sensors*, 20(6):1803, 2020. Number: 6 Publisher: Multidisciplinary Digital Publishing Institute.
- [58] JA Covington et al. Combined smart chemfet/resistive sensor array. In *SENSORS, 2003 IEEE*, volume 2, pages 1120–1123. IEEE, 2003.
- [59] Andrzej G Lozowski et al. Signal processing with temporal sequences in olfactory systems. *IEEE Transactions on neural networks*, 15(5):1268–1275, 2004.
- [60] Nestor Caticha et al. Computational capacity of an odorant discriminator: The linear separability of curves. *Neural computation*, 14(9):2201–2220, 2002.
- [61] Jiawei Zhao, Andy Q. Chen, Jaewook Ryu, and Josefina del Marmol. Structural basis of odor sensing by insect heteromeric odorant receptors. *Science*, 384(6703):1460–1467, 2024.
- [62] Walton D Jones, Thuy-Ai T Nguyen, Brian Kloss, Kevin J Lee, and Leslie B Vosshall. Functional conservation of an insect odorant receptor gene across 250 million years of evolution. *Current Biology*, 15(4):R119–R121, 2005.
- [63] Dingquan Yu, Grzegorz Chojnowski, Maria Rosenthal, and Jan Kosinski. Alphapulldown—a python package for protein–protein interaction screens using alphafold-multimer. *Bioinformatics*, 39(1):btac749, 2023.
- [64] John Jumper, Richard Evans, Alexander Pritzel, Tim Green, Michael Figurnov, Olaf Ronneberger, Kathryn Tunyasuvunakool, Russ Bates, Augustin Židek, Anna Potapenko, et al. Highly accurate protein structure prediction with alphafold. *nature*, 596(7873):583–589, 2021.
- [65] Richard Evans, Michael O’Neill, Alexander Pritzel, Natasha Antropova, Andrew Senior, Tim Green, Augustin Židek, Russ Bates, Sam Blackwell, Jason Yim, et al. Protein complex prediction with alphafold-multimer. *bioRxiv*, pages 2021–10, 2021.
- [66] Johannes Kraml, Anna S Kamenik, Franz Waibl, Michael Schauerperl, and Klaus R Liedl. Solvation free energy as a measure of hydrophobicity: application to serine protease binding interfaces. *Journal of chemical theory and computation*, 15(11):5872–5882, 2019.
- [67] Joel A. Butterwick, Josefina del Marmol, Kelly H. Kim, Martha A. Kahlson, Jackson A. Rogow, Thomas Walz, and Vanessa Ruta. Cryo-em structure of the insect olfactory receptor orco. *Nature*, 560(7719):447–452, Aug 2018.
- [68] Yidong Wang, Liang Qiu, Bing Wang, Zeyuan Guan, Zhi Dong, Jie Zhang, Song Cao, Lulu Yang, Bo Wang, Zhou Gong, et al. Structural basis for odorant recognition of the insect odorant receptor or-orco heterocomplex. *Science*, 384(6703):1453–1460, 2024.

- [69] Jiawei Zhao, Andy Q Chen, Jaewook Ryu, and Josefina Del Marmol. Structural basis of odor sensing by insect heteromeric odorant receptors. *Science*, 384(6703):1460–1467, 2024.
- [70] C. Giovanni Galizia, Daniel Munch, Martin Strauch, Anja Nissler, and Shouwen Ma. Integrating heterogeneous odor response data into a common response model: A door to the complete olfactome. *Chemical Senses*, 35(7):551–563, 06 2010.
- [71] Daniel Munch and C. Giovanni Galizia. DoOR 2.0 - comprehensive mapping of drosophila melanogaster odorant responses. *Sci Rep*, 6(1):21841, 2016. Publisher: Nature Publishing Group.
- [72] Marcus C. Stensmyr, Hany K.M. Dweck, Abu Farhan, Irene Ibba, Antonia Strutz, Latha Mukunda, Jeanine Linz, Veit Grabe, Kathrin Steck, Sofia Lavista-Llanos, Dieter Wicher, Silke Sachse, Markus Knaden, Paul G. Becher, Yoichi Seki, and Bill S. Hansson. A conserved dedicated olfactory circuit for detecting harmful microbes in drosophila. *Cell*, 151(6):1345–1357, December 2012.
- [73] Elissa A Hallem, Michael G Ho, and John R Carlson. The molecular basis of odor coding in the drosophila antenna. *Cell*, 117(7):965–979, June 2004.
- [74] Aaron L. Goldman, Wynand Van der Goes van Naters, Derek Lessing, Coral G. Warr, and John R. Carlson. Coexpression of two functional odor receptors in one neuron. *Neuron*, 45(5):661–666, March 2005.
- [75] Daniela Pelz, Tina Roeske, Zainulabeuddin Syed, Marien de Bruyne, and C. Giovanni Galizia. The molecular receptive range of an olfactory receptor in vivo (drosophila melanogaster or22a). *Journal of Neurobiology*, 66(14):1544–1563, November 2006.
- [76] C. Andrea Yao, Rickard Ignell, and John R. Carlson. Chemosensory coding by neurons in the coeloconic sensilla of the drosophila antenna. *The Journal of Neuroscience*, 25(37):8359–8367, September 2005.
- [77] Elissa A. Hallem and John R. Carlson. Coding of odors by a receptor repertoire. *Cell*, 125(1):143–160, April 2006.
- [78] Stephanie Lynn Turner and Anandasankar Ray. Modification of co2 avoidance behaviour in drosophila by inhibitory odorants. *Nature*, 461(7261):277–281, August 2009.
- [79] C. Giovanni Galizia, Daniel Munch, Martin Strauch, Anja Nissler, and Shouwen Ma. Integrating heterogeneous odor response data into a common response model: A door to the complete olfactome. *Chemical Senses*, 35(7):551–563, June 2010.
- [80] B. Marshall, C. G. Warr, and M. de Bruyne. Detection of volatile indicators of illicit substances by the olfactory receptors of drosophila melanogaster. *Chemical Senses*, 35(7):613–625, June 2010.
- [81] Ana F. Silbering, Raphael Rytz, Yael Grosjean, Liliane Abuin, Pavan Ramdya, Gregory S. X. E. Jefferis, and Richard Benton. Complementary function and

- integrated wiring of the evolutionarily distinct drosophila olfactory subsystems. *The Journal of Neuroscience*, 31(38):13357–13375, September 2011.
- [82] Hany K.M. Dweck, Shimaa A.M. Ebrahim, Sophie Kromann, Deni Bown, Ylva Hillbur, Silke Sachse, Bill S. Hansson, and Marcus C. Stensmyr. Olfactory preference for egg laying on citrus substrates in drosophila. *Current Biology*, 23(24):2472–2480, December 2013.
- [83] Stephan Gabler, Jan Soelter, Taufia Hussain, Silke Sachse, and Michael Schmuker. Physicochemical vs. vibrational descriptors for prediction of odor receptor responses. *Molecular Informatics*, 32(9–10):855–865, October 2013.
- [84] David S. Ronderos, Chun-Chieh Lin, Christopher J. Potter, and Dean P. Smith. Farnesol-detecting olfactory neurons in drosophila. *The Journal of Neuroscience*, 34(11):3959–3968, March 2014.
- [85] Hany K. M. Dweck, Shimaa A. M. Ebrahim, Michael Thoma, Ahmed A. M. Mohamed, Ian W. Keeseey, Federica Trona, Sofia Lavista-Llanos, Aleš Svatoš, Silke Sachse, Markus Knaden, and Bill S. Hansson. Pheromones mediating copulation and attraction in drosophila. *Proceedings of the National Academy of Sciences*, 112(21), May 2015.
- [86] Marien de Bruyne, Peter J. Clyne, and John R. Carlson. Odor coding in a model olfactory organ: The *Drosophila* maxillary palp. *J. Neurosci.*, 19(11):4520–4532, 1999. Society for Neuroscience.
- [87] Marien de Bruyne, Kara Foster, and John R. Carlson. Odor coding in the *Drosophila* antenna. *Neuron*, 30(2):537–552, 2001.
- [88] Scott A. Kreher, Jae Young Kwon, and John R. Carlson. The molecular basis of odor coding in the *Drosophila* larva. *Neuron*, 46(3):445–456, 2005.
- [89] Wynand van der Goes van Naters and John R. Carlson. Receptors and neurons for fly odors in drosophila. *Current Biology*, 17(7):606–612, 2007. Publisher: Elsevier.
- [90] Scott A. Kreher, Dennis Mathew, Junhyong Kim, and John R. Carlson. Translation of sensory input into behavioral output via an olfactory system. *Neuron*, 59(1):110–124, 2008. Publisher: Elsevier.
- [91] Marien de Bruyne, Renee Smart, Elizabeth Zammit, and Coral G. Warr. Functional and molecular evolution of olfactory neurons and receptors for aliphatic esters across the drosophila genus. *Journal of Comparative Physiology A*, 196(2):97–109, 2010.
- [92] Marcus C. Stensmyr, Hany K. M. Dweck, Abu Farhan, Irene Ibba, Antonia Strutz, Latha Mukunda, Jeanine Linz, Veit Grabe, Kathrin Steck, Sofia Lavista-Llanos, Dieter Wicher, Silke Sachse, Markus Knaden, Paul G. Becher, Yoichi Seki, and Bill S. Hansson. A conserved dedicated olfactory circuit for detecting harmful microbes in drosophila. *Cell*, 151(6):1345–1357, 2012. Publisher: Elsevier.
- [93] Jan Steinkühler, Jaime Agudo-Canalejo, Reinhard Lipowsky, and Rumiana

- Dimova. Modulating vesicle adhesion by electric fields. *Biophysical Journal*, 111(7):1454–1464, 2016.
- [94] Oskar Staufer, Jacqueline A De Lora, Eleonora Bailoni, Alisina Bazrafshan, Amelie S Benk, Kevin Jahnke, Zachary A Manzer, Lado Otrin, Telmo Díez Pérez, Judee Sharon, Jan Steinkühler, Katarzyna P Adamala, Bruna Jacobson, Marileen Dogterom, Kerstin Göpfrich, Darko Stefanovic, Susan R Atlas, Michael Grunze, Matthew R Lakin, Andrew P Shreve, Joachim P Spatz, and Gabriel P López. Science forum: Building a community to engineer synthetic cells and organelles from the bottom-up. *eLife*, 10:e73556, dec 2021.
- [95] Jason K Eshraghian, Max Ward, Emre O Neftci, Xinxin Wang, Gregor Lenz, Girish Dwivedi, Mohammed Bennamoun, Doo Seok Jeong, and Wei D Lu. Training spiking neural networks using lessons from deep learning. *Proceedings of the IEEE*, 2023.
- [96] Alexander Egea-Weiss, Christoph J Kleineidam, Paul Szyszka, et al. High precision of spike timing across olfactory receptor neurons allows rapid odor coding in drosophila. *IScience*, 4:76–83, 2018.
- [97] Radoslav Krivák and David Hoksza. P2rank: machine learning based tool for rapid and accurate prediction of ligand binding sites from protein structure. *Journal of cheminformatics*, 10:1–12, 2018.
- [98] Oleg Trott and Arthur J Olson. Autodock vina: improving the speed and accuracy of docking with a new scoring function, efficient optimization, and multithreading. *Journal of computational chemistry*, 31(2):455–461, 2010.
- [99] Rolf Weis and Peter Fromherz. Frequency dependent signal transfer in neuron transistors. *Phys. Rev. E*, 55:877–889, Jan 1997.
- [100] Kevin Max, Larissa Sames, Shimeng Ye, Jan Steinkühler, and Federico Corradi. Code repository for Synthetic Biology Meets Neuromorphic Computing: Towards a Bio-Inspired Olfactory Perception System. <https://doi.org/10.5281/zenodo.15110986>.
- [101] R Sanjay, V Senthil Rajan, and B Venkataramani. A low-power low-noise and high swing biopotential amplifier in 0.18 μm cmos. *Analog Integrated Circuits and Signal Processing*, 96:565–576, 2018.
- [102] Chiara Bartolozzi and Giacomo Indiveri. Synaptic dynamics in analog vlsi. *Neural computation*, 19(10):2581–2603, 2007.
- [103] Giacomo Indiveri, Bernabé Linares-Barranco, Tara Julia Hamilton, André van Schaik, Ralph Etienne-Cummings, Tobi Delbruck, Shih-Chii Liu, Piotr Dudek, Philipp Häfliger, Sylvie Renaud, et al. Neuromorphic silicon neuron circuits. *Frontiers in neuroscience*, 5:73, 2011.
- [104] Ning Qiao and Giacomo Indiveri. Analog circuits for mixed-signal neuromorphic computing architectures in 28 nm fd-soi technology. In *2017 IEEE SOI-3D-*

- Subthreshold Microelectronics Technology Unified Conference (S3S)*, pages 1–4. IEEE, 2017.
- [105] Hossein Eslahi, Tara J Hamilton, and Sourabh Khandelwal. Compact and energy efficient neuron with tunable spiking frequency in 22-nm fdsoi. *IEEE Transactions on Nanotechnology*, 21:189–195, 2022.